

This is an Open Access document downloaded from ORCA, Cardiff University's institutional repository: <https://orca.cardiff.ac.uk/id/eprint/138961/>

This is the author's version of a work that was submitted to / accepted for publication.

Citation for final published version:

Zhou, Dong, Abass, Ahmed, Lopes, Bernardo, Eliasy, Ashkan, Hayes, Sally, Boote, Craig, Meek, Keith M., Movchan, Alexander, Movchan, Natalia and Elsheikh, Ahmed 2021. Fibril density reduction in keratoconic corneas. *Journal of the Royal Society Interface* 18 (175), 20200900. 10.1098/rsif.2020.0900

Publishers page: <http://dx.doi.org/10.1098/rsif.2020.0900>

Please note:

Changes made as a result of publishing processes such as copy-editing, formatting and page numbers may not be reflected in this version. For the definitive version of this publication, please refer to the published source. You are advised to consult the publisher's version if you wish to cite this paper.

This version is being made available in accordance with publisher policies. See <http://orca.cf.ac.uk/policies.html> for usage policies. Copyright and moral rights for publications made available in ORCA are retained by the copyright holders.



Fibril Density Reduction in Keratoconic Corneas

Dong Zhou¹, Ahmed Abass^{2*}, Bernardo Lopes^{2,3}, Ashkan Eliasy², Sally Hayes⁴, Craig Boote⁴, Keith M Meek⁴, Alexander Movchan¹, Natalia Movchan¹, Ahmed Elsheikh^{2, 5, 6}

¹ Department of Mathematical Sciences, University of Liverpool, Liverpool, UK

² School of Engineering, University of Liverpool, Liverpool, UK

³ Department of Ophthalmology, Federal University of Sao Paulo – Sao Paulo

⁴ School of Optometry and Vision Sciences, Cardiff University, Cardiff, UK

⁵ Beijing Advanced Innovation Centre for Biomedical Engineering, Beihang University, Beijing, 100083, China

⁶ NIHR Biomedical Research Centre for Ophthalmology, Moorfields Eye Hospital NHS Foundation Trust and UCL Institute of Ophthalmology, London, UK

***Corresponding author:** Dr Ahmed Abass, School of Engineering, University of Liverpool, Liverpool, UK, a.abass@liverpool.ac.uk

Keywords: cornea; keratoconus; tissue microstructure; ocular biomechanics

Word count: 5279

26 **Abstract**

27 This study aims to estimate the reduction in collagen fibril density within the central 6mm
28 radius of keratoconic corneas through processing of microstructure and videokeratography
29 data. Collagen fibril distribution maps and topography maps were obtained for seven
30 keratoconic and six healthy corneas, and topographic features were assessed to detect and
31 calculate the area of the cone in each keratoconic eye. The reduction in collagen fibril density
32 within the cone area was estimated with reference to the same region in the characteristic
33 collagen fibril maps of healthy corneas. Together with minimum thickness and mean central
34 corneal refractive power, the cone area was correlated with the reduction in the cone collagen
35 fibrils. For the corneas considered, the mean area of keratoconic cones was 3.30 ± 1.90 mm².
36 Compared with healthy corneas, fibril density in the cones of keratoconic corneas was lower
37 by as much as 35% and the mean reduction was $17 \pm 10\%$. A linear approximation was
38 developed to relate the magnitude of reduction to the refractive power, minimum corneal
39 thickness and cone area ($R^2 = 0.95$, $p < 0.001$). Outside the cone area, there was no significant
40 difference between fibril arrangement in healthy and keratoconic corneas. The presented
41 method can predict the mean fibril density in the keratoconic eye's cone area. The technique
42 can be applied in microstructure-based finite element models of the eye to regulate its stiffness
43 level and the stiffness distribution within the areas affected by keratoconus.

44

45 **Introduction**

46 Keratoconus (KC) is a bilateral non-inflammatory corneal disease that affects approximately
47 1 in 2000 of the population (1). The keratoconic cornea progressively develops ectasia with
48 local thinning and a cone-shaped protrusion, which results in visual impairment. The
49 management of KC, including its diagnosis and treatment, has developed significantly in
50 recent decades.

51 Computer-assisted videokeratography provides quantitative imaging of corneal anterior and
52 posterior topographies. KC can be detected and classified based on corneal topography
53 through clinical signs of disease evolution, index-based classification systems and advanced
54 machine learning algorithms (1-7). These detection techniques are clinically useful to evaluate
55 the stage of KC and guide the selection of suitable treatments.

56 Corneal shape is the outcome of an equilibrium between the intraocular pressure (IOP) and
57 the mechanical resistance (or stiffness) of ocular tissue. In keratoconic eyes, and in particular
58 within the KC cone, the stiffness of corneal tissue is known to be lower than in healthy corneas
59 due to the combined effect of smaller thickness and softer material (8-12). The reduced
60 stiffness in the cone is thought to be the cause of the distortion of the tissue and the
61 subsequent loss in vision clarity.

62 While the pathogenesis of KC remains unclear, there is strong evidence that the
63 microstructural alterations in cone tissue, in terms of both collagen fibril density and
64 organisation, are behind the reduced stiffness of KC tissue. Literature in this field shows
65 consistently that healthy corneas have preferential fibril organisation with more fibrils lying in
66 the horizontal and vertical directions than in any other direction in the central region of the
67 cornea; the fibrils then gradually assume an increasingly tangential arrangement with
68 increasing proximity to the limbus (13-15). This arrangement is clearly disturbed in KC eyes
69 and is accompanied by a significant reduction in fibril content (16-18), and a decreased
70 incidence of collagen interlacing between lamellae in the para-apical region (19, 20). These
71 changes cause loss of mechanical cohesiveness, and facilitate slippage between stromal

72 lamellae (16, 21). Hayes, Boote (18) demonstrated that these effects were concentrated in the
73 area where the KC cone develops with significant local thinning and surface distortion, thus
74 providing evidence of an association between microstructural degradation and topographical
75 distortion.

76 The last two decades saw several attempts to develop numerical models of ocular
77 biomechanical behaviour based on the tissue's microstructure and in particular its collagen
78 fibril distribution. These models benefitted from the extensive work carried out in X-ray
79 scattering studies to quantify the fibril density and orientation across the cornea (22-26).
80 However, while similar studies have attempted to quantify the microstructural features of KC
81 corneas, no consensus has developed yet on the effect of KC on fibril organisation.

82 This study attempts to address this shortfall through analysis of microstructure maps of seven
83 KC corneas and six healthy corneas. It seeks to provide an estimate of the reduction in fibril
84 density within the cone area that can be expected in eyes with different disease severity stages,
85 thickness loss and cone surface areas. With this information, progress can be made in building
86 patient-specific, microstructure-based numerical models of the biomechanical behaviour of
87 KC eyes.

88

89 **Methods**

90 **Collagen fibril maps**

91 This study utilised a large collection of previously published x-ray scattering data that was
92 gathered for a number of individual studies (15, 27-29), and done so in accordance with the
93 ethical principles of the declaration of Helsinki and its subsequent revisions, with full, informed
94 consent from the human tissue donors, and with approval from the Human Science Ethical
95 Committee (School of Optometry and Vision Sciences, Cardiff University, UK). This study
96 involved 6 healthy donor corneas (with at least 13 mm of surrounding sclera), collected post-
97 mortem from 4 donors aged between 54 and 75 years. It also included 7 central corneal
98 buttons with severe keratoconus (KC) collected using 7.5 mm diameter trephines from 7

99 donors aged between 24 and 39 years who underwent penetrating keratoplasty. The patients'
100 demographic characteristics and corneal thickness values are summarised in Table 1.

101

102 Table 1 Patients' demographic characteristics including age, gender, left/right eyes.

	Healthy	Keratoconus	
Number of corneas and donors	6, 4	7, 7	
Age in years (mean±SD range)	65.0±8.8 (54 – 75)	30.1±4.4 (24 – 39)	p < 0.001
Left:Right eyes ratio	1.0:1.0	1.0:2.5	p = 0.576
Male:Female gender ratio	1:1	1:1.3	p = 1.000
Central corneal thickness (mean±std μm)	546.4±12.5	293.7±88.2	p < 0.001

103

104

105 The healthy corneas were obtained within 18 hrs post-mortem, stored at 4°C for transport and
106 subsequently fixed in 4% PFA prior to scanning by wide-angle x-ray scattering (WAXS), while
107 the KC corneas were obtained post-operatively, quickly frozen in liquid Nitrogen and stored at
108 -80°C until required for data collection. This difference in tissue preparation methods was
109 found earlier to have no significant effect on WAXS data (30).

110 Thickness measurements were taken in healthy eyes prior to PFA tissue fixation using an
111 ultrasound pachymeter (Pachmate 55; DGH Technologies, Exton, PA) with $\pm 5 \mu\text{m}$ accuracy
112 (Table 1). The thickness was measured at the centre of each cornea and at intervals of 2.5
113 mm along 8 meridians. Measurements were taken 3 times at each point and the mean value
114 was used. Recorded standard deviation was less than 10 μm for all pachymetry thickness
115 measurements. Interpolation between these values was then used to estimate the tissue
116 thickness throughout the corneal surface. On the other hand, the thickness across the surface
117 of keratoconic corneas was obtained directly from the videokeratography images recorded
118 prior to the penetrating keratoplasty (Table 1). The different methods used to measure the
119 thickness were found in the past to produce similar results, and were therefore not expected
120 to make a notable effect on the results of this study (31, 32).

121 Based on the measured central corneal thickness of the healthy specimens (530-560 μm) and
122 the known relationship between thickness and hydration, the healthy corneas were deemed

123 to be close to physiological hydration at the time of data collection, and therefore at similar
124 hydration to that of the keratoconus tissue.

125

126 The white-to-white (WTW) distance was measured in healthy eyes by a digital calliper
127 (Mitutoyo, Hampshire, UK) with $\pm 20 \mu\text{m}$ accuracy, while in keratoconic eyes, it was obtained
128 directly from the Orbscan output. The WTW values showed little variation with a mean,
129 standard deviation and range of 12.11 ± 0.46 (11.8-13.1 mm) for all eyes. However, despite
130 this little variation, the sampling distance within every specimen was normalised such that the
131 WTW distance became 12.11 mm.

132

133 Due to the large dimensions of the healthy cornea-scleral specimens relative to the size of the
134 specimen holder, it was necessary to flatten the tissue slightly prior to scanning. This was
135 achieved by performing a series of six meridional incisions, extending from the corneal limbus
136 to the outer edge of the sclera (thus avoiding damage to the cornea itself) (15, 27).

137 Just before testing, the KC corneas were thawed, and both the healthy and KC tissue was
138 wrapped in polyvinylidene chloride catering film to minimise tissue dehydration. Wide angle x-
139 rays scatter (WAXS) patterns were obtained from each specimen in a grid system of 0.5 mm
140 intervals in both horizontal and vertical directions for healthy eyes (27), and 0.25 mm intervals
141 for KC eyes (29). The x-ray scattering images collected at every scanning spot were
142 normalised against the x-ray beam intensity and the x-ray exposure time, and subsequently
143 analysed to determine the orientation of fibrillar collagen at equally-spaced 256 orientations
144 covering 360° , as well as the total collagen x-ray scatter intensity at each sampling position.

145 Assuming hydration is fairly uniform across the cornea, then the total x-ray scattering intensity
146 can be seen as a reasonable representation of the relative mass of collagen at each sampling
147 site within an individual cornea. Fibril density was calculated as the total x-ray scatter intensity
148 divided by the local tissue thickness.

149

150 Due to the potential for tissue distortion artefacts close to the cut edges in both the healthy
151 and keratoconus specimens, data obtained within 0.75 mm of the sample edge was excluded
152 from the analysis.

153

154 **Identification of cone area in KC corneas**

155 Videokeratography scans of the keratoconic buttons were obtained using Orbscan (Bausch &
156 Lomb, Technolas PV, Germany) before the surgery, in which they were removed. These scans
157 provided corneal anterior and posterior topography maps, mean power maps and thickness
158 distribution maps. **Central corneal thickness measurements with partial coherence**
159 **interferometry, ultrasound, and the Orbscan system (33).** The topography maps enabled
160 calculation of the height of the cornea relative to a best-fit spherical surface, with the highest
161 point assumed to represent the centre of the keratoconic cone (34, 35). **The refractive power**
162 **P was calculated using the Gaussian optics formula (36-38).**

$$P = \frac{n_{\text{cornea}} - n_{\text{air}}}{R_{\text{anterior}}} + \frac{n_{\text{aqueous}} - n_{\text{cornea}}}{R_{\text{posterior}}} - \frac{t_c}{n_{\text{cornea}}} \times \frac{n_{\text{cornea}} - n_{\text{air}}}{R_{\text{anterior}}} \times \frac{n_{\text{aqueous}} - n_{\text{cornea}}}{R_{\text{posterior}}} \quad (1)$$

163 **Where the refractive indices of air, n_{air} , cornea, n_{cornea} , and aqueous, n_{aqueous} , were set at**
164 **1.0, 1.376 and 1.336, respectively following Gullstrand's relaxed eye model (39, 40), and t_c ,**
165 **represented the central corneal thickness. The sagittal radii of curvatures at any point were**
166 **calculated as:**

$$R = \frac{x}{\cos\left(\frac{\pi}{2} - \alpha\right)} \quad (2)$$

167 **where α is the tangent angle at the calculation point and x is the distance from the apex.**

168 The mean power map was constructed based on the average of the two principal curvatures
169 at each scanned point (38).

170

171 The boundary of keratoconic cones was detected based on the observation that it coincided
172 with a sudden, abnormal reversal of corneal curvature. As outlined in our earlier studies (35,
173 41, 42), corneal profiles along equally-spaced meridian lines originating at the cone centre

174 and extending outwards were analysed. Initially, a sphere was fitted to the central, 8 mm
175 diameter area of each corneal anterior surface, and the radial distance from each data point
176 on a corneal surface to the centre of the sphere was calculated. This was followed by
177 subtracting the radius of the sphere from these radial distances and the position and
178 magnitude of the largest positive difference were assumed to point at the location and height
179 of the cone centre, respectively.

180 To estimate the area of pathology, height data relative to the optimal sphere were determined
181 along 360 equally-spaced lines meeting at the cone centre and extending outwards using
182 triangle-based cubic interpolation (43). A first derivative of the height data was calculated to
183 determine the tangent to the surface along these lines. The second derivative was then
184 calculated to represent the rate of change of this gradient. Since the rate of gradient change
185 experiences a change in direction when the point of interest moves from the cone area to the
186 surrounding healthy area, a sudden change in the sign of the rate of change in tangent
187 gradient is indicative of an intersection with the transition zone between the pathologic area
188 and the remaining corneal tissue. Locating the transition zone between the area of pathology
189 and the remaining corneal tissue using this method then allowed calculating the cone area.

190 An iterative process was then initiated in which the cone area was removed from the
191 topography data before re-identifying the optimal sphere and repeating the subsequent steps.
192 This process was repeated until the difference between the results (cone height and centre
193 location) of two subsequent analyses became smaller than 1.0 μm .

194

195 **Fibril density reduction factor ' κ '**

196 Assessment of the reduction in collagen fibril density in KC cones started with developing a
197 map representing the mean density distribution in the six healthy corneas scanned. As it was
198 not possible to scan at exactly the same points in all cornea specimens, as discussed in our
199 previous study Zhou, Eliasy (15), 10th order Zernike polynomials were used to fit the fibril

200 density measurements obtained for each cornea. The average values of Zernike coefficients
201 were then determined and used to represent the mean density distribution for healthy corneas.
202 This process enabled comparison of fibril density in KC corneas (both within and outside cone
203 boundary) with mean fibril density in the corresponding areas of healthy corneas. Therefore,
204 the analysis included two sets of comparisons. First, the fibril density within the cone area in
205 keratoconic corneas was compared to the density in corresponding areas in healthy corneas.
206 The second comparison was between the fibril density outside the cone in keratoconic corneas
207 and the density in corresponding areas in healthy eyes. This exercise led to the development
208 of a fibril density reduction factor (κ) that quantified the mean reduction in fibril density in each
209 KC cone relative to the corresponding area in healthy corneas:

$$\kappa = \frac{C_k S_h}{C_h S_k} \quad (3)$$

210 where, for each KC cone, C_h and S_h are the mean fibril density in the healthy corneal areas
211 that correspond to the areas inside (C) and outside (S) the KC cone, respectively. Likewise,
212 C_k and S_k represent the mean fibril density inside and outside the cone area in each KC cornea.

213 Expressing the fibril reduction factor as a ratio was used to eliminate any hydration-induced
214 variation in absolute collagen scatter caused by the different sample storage methods of KC
215 and healthy corneal specimens.

216 A stepwise linear regression model was fitted to assess the correlation between κ and
217 topographic features of the cornea including the mean central refractive power (P) obtained
218 within the central 3mm diameter zone, the minimum corneal thickness (T), the KC cone area
219 (A) and the distance between the cone centre and corneal apex (D). Both P and T were
220 extracted from the Obscan reports. Using the forward stepwise approach, the variables that
221 could explain most of the variance in κ and therefore composed the final model were P, T and
222 A.

223 The first-order polynomial adopted for the dependence of κ on P, T and A took the following
224 form (the first order was adopted to avoid overfitting, which can be caused by the small size
225 of the database):

$$\kappa = a_1A + a_2P + a_3T + a_4 \quad (4)$$

226 In Equation 4, a_1 to a_4 are constants, which were optimised using the least square method
 227 with the objective function:

$$\text{RMS} = \frac{1}{n} \sum_{i=1}^n (\kappa_{mi} - \kappa_e(A_i, P_i, T_i))^2 \quad (5)$$

228 Where RMS is the root mean square error, n is the number of data points, κ_{mi} is the measured
 229 value of density reduction based on KC fibril map i , and κ_e is the estimated density reduction
 230 based on Equation 4. Each KC cornea provided one data point i , and six more points were
 231 added to represent the healthy corneas, with $\kappa = 1$, $A = 0$, $P \in [43D, 45D]$, $T \in$
 232 $[530\mu\text{m}, 560\mu\text{m}]$.

233 **K-fold cross-validation was used to test the accuracy of the linear model in predicting fibril**
 234 **density reduction. Data of one keratoconic cornea was kept in every validation cycle to be**
 235 **used in testing the regression model, while data of other eyes were used in its training and**
 236 **calculating its coefficients. The model finally adopted the average values of coefficients**
 237 **following all K-fold cross-validation steps.**

238 **Statistical analysis**

239 Statistical analysis was carried out using the MATLAB and Statistics Toolbox Release 2019b
 240 (The MathWorks, Inc., Natick, Massachusetts, United States). The Goodness-of-fit of the
 241 regression model relating κ to P , T and A was evaluated with the coefficient of determination
 242 (R^2). The closer the R^2 is to 1, the higher the variation of the dependent variable explained by
 243 the independent variables in the regression model. The comparison of the continuous
 244 variables was performed using either Student's t-test or Mann-Whitney U-test according to the
 245 variables' distribution. The categorical variables were compared using the Chi-Squared test.
 246 A p-value lower than 0.050 was considered statistically significant.

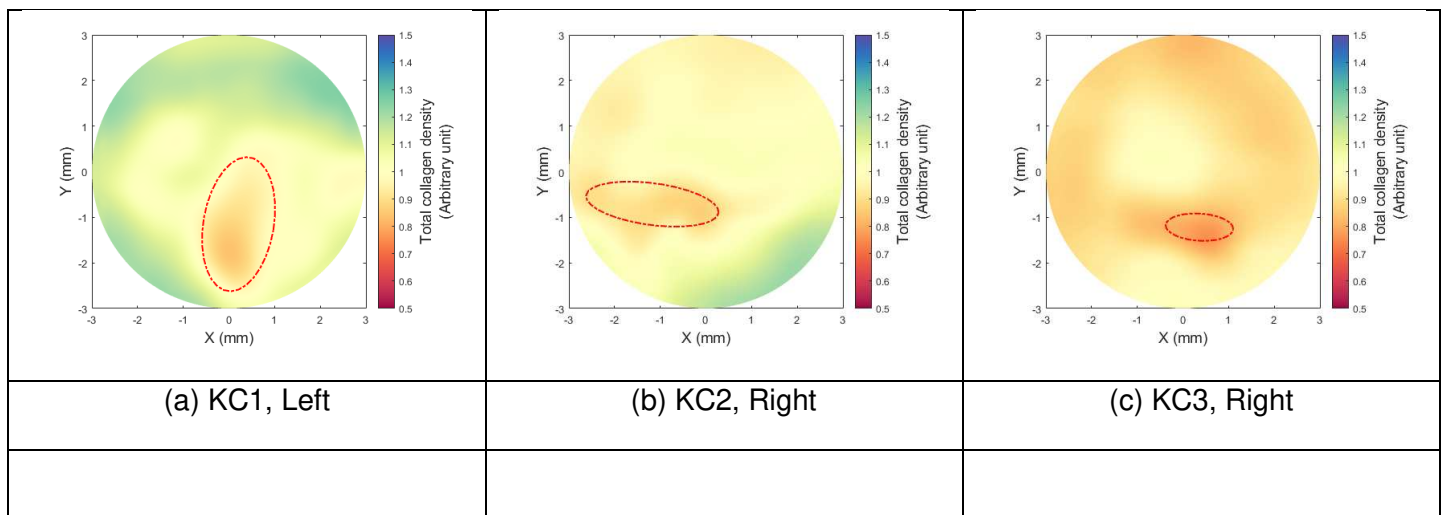
247

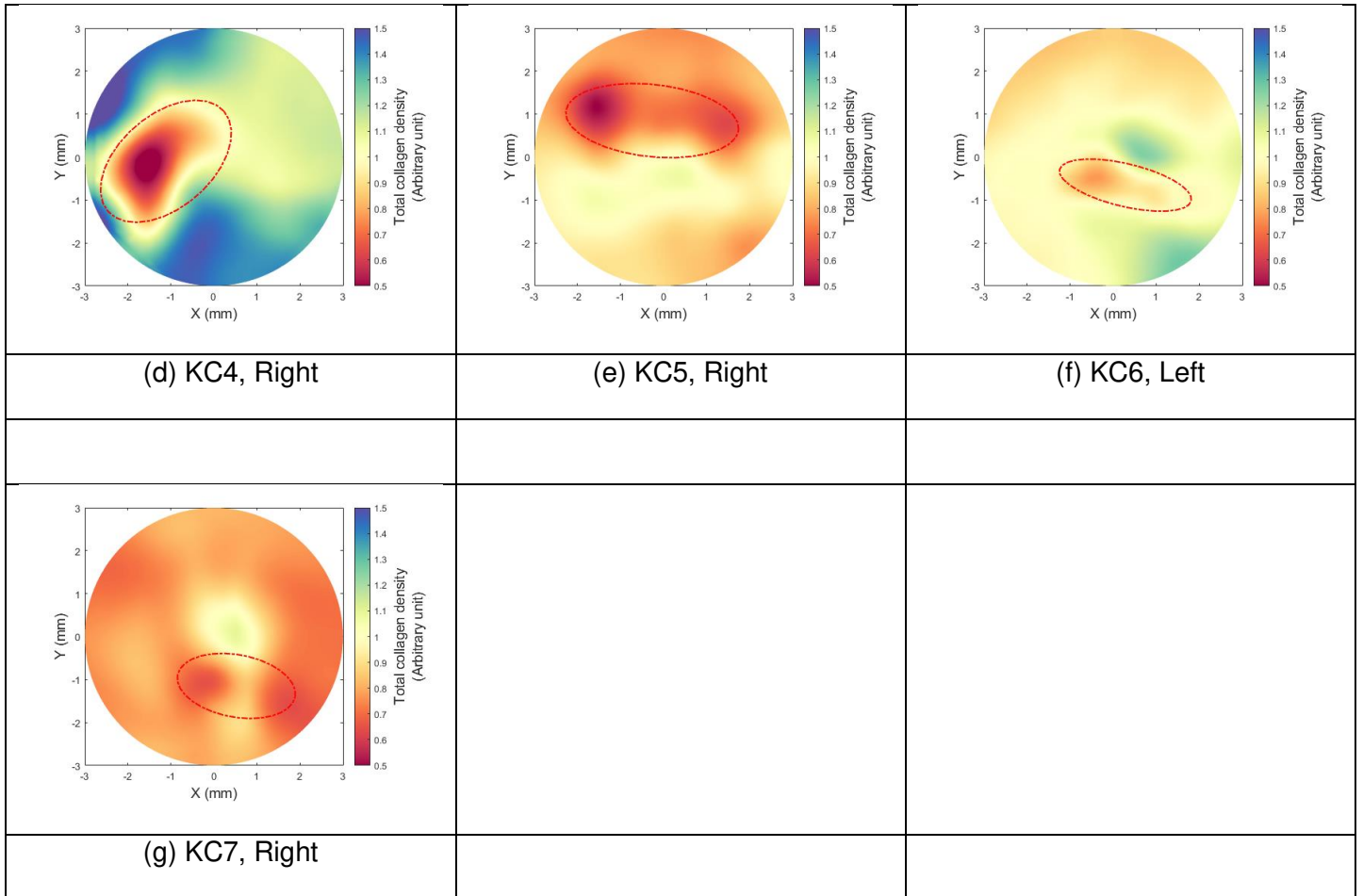
248 **Results**

249 **KC cone area**

250 Figure 1 shows the fibril density maps of the seven keratoconic corneas with the estimated
 251 cone boundary marked in each case. The cone area (A), the central refractive power (P), the
 252 minimum thickness (T), and the fibril reduction factor (κ) measured from the fibril density maps
 253 are also listed in Table 2. The results show trends in which increases in cone area or mean
 254 power, or decreases in min thickness were associated with higher fibril density reductions (i.e.
 255 smaller κ). However, despite the significant correlation between κ and each of A, P and T,
 256 there was no correlation between A and P ($p= 0.37$), A and T ($p= 0.89$), or R and T ($p= 0.18$).

257
 258
 259
 260
 261
 262
 263
 264





265 Figure 1 Fibril density maps for seven keratoconic corneas. S, I, T and N indicate superior,
 266 inferior, temporal and nasal directions, respectively. The origin (0,0) is the corneal apex. Red
 267 lines represent the KC cone boundaries.

268

269

270 Table 2 Measurements of cone area, mean central refractive power, minimum thickness and
 271 cone fibril density reduction in keratoconic corneas

Specimen	Cone area, A (mm ²)	Mean power, P (Diopter)	Min Thickness, T (μm)	Fibril reduction factor, κ
KC1	3.61	46.90	483.0	0.84
KC2	2.18	49.20	220.0	0.90
KC3	0.72	54.30	298.0	0.91
KC4	6.24	58.30	277.0	0.65
KC5	5.17	59.30	279.0	0.73
KC6	2.07	63.20	227.0	0.89
KC7	3.12	63.20	272.0	0.87
Mean±SD	3.30±1.90	56.34±6.47	293.7±88.2	0.83±0.10

(min-max)	(0.72-6.24)	(46.90-63.20)	(220.0-483.0)	(0.65-0.91)
-----------	-------------	---------------	---------------	-------------

272

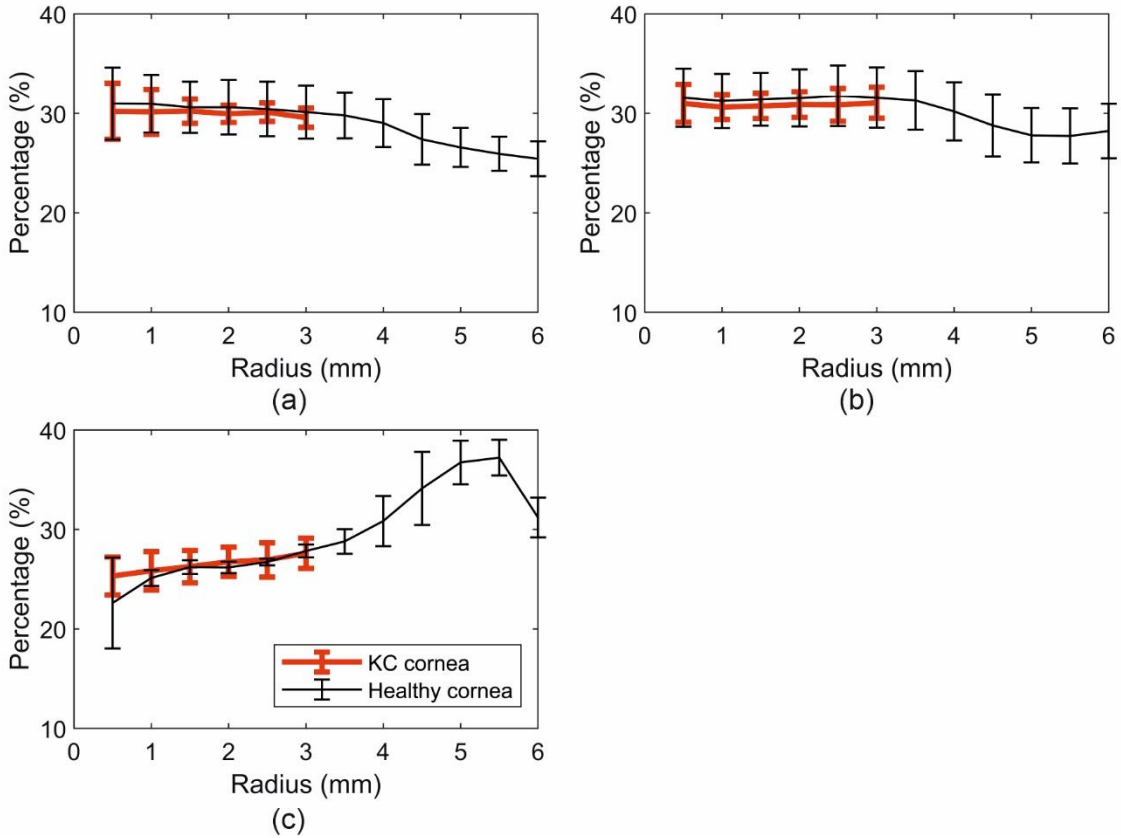
273

274 **Fibril distribution comparisons**

275 The effect of KC on fibril distribution outside the cone area was studied with reference to the
276 results in Figure 2. In this figure, the proportion of collagen fibrils in the 45° sectors surrounding
277 the horizontal and vertical directions, and the tangential direction to the cornea edge was
278 quantified within successive tissue rings, each with 0.5 mm width. All the x-ray scanning points
279 in the healthy cornea maps were included in the calculations while the cone areas were
280 excluded from the KC cornea calculations. The results covered the central zones with 3 mm
281 radius in KC corneas and 6 mm radius in healthy corneas.

282 The central corneas within 3 mm radius had percentages of horizontal and vertical fibril
283 contents between 30% and 35% of total density in both healthy and KC eyes. **No significant**
284 **differences were found in percentages of preferentially aligned horizontal fibrils (p= 0.29) or**
285 **vertical fibrils (p= 0.22) between healthy and KC corneas. Similarly, there were no significant**
286 **differences between healthy and KC corneas in the percentages of tangential fibrils – mean**
287 **values ranged between 24 and 28% in both specimen groups.**

288



289

290 Figure 2 Percentage of fibril quantity in (a) the horizontal direction, (b) the vertical direction,
 291 and (c) the tangential direction in healthy and keratoconic cornea specimens.

292

293

294 **Fibril density reduction factor ‘ κ ’**

295 Values of constants a_1 to a_4 in the linear relationship between κ and A, P and T, were
 296 determined using the least square method as:

$$\kappa = -0.0425A - 0.0004P + 0.0001T + 0.9727 \quad (6)$$

297 The relationship reflected a decrease in κ (denoting a larger fibril density reduction) with lower
 298 minimum corneal thickness (T) ($p=0.015$), larger central refractive power (P) ($p=0.003$) and
 299 larger cone area (A) ($p<0.001$). The R^2 -value was 0.95 ($p<0.001$) and indicated the strong fit
 300 of Equation 6 to the measured fibril density measurements. The K-fold cross-validation
 301 showed 2.00% error in average fibril reduction in training the model and 2.58% in its testing.

302

303 Discussion

304 Microstructural abnormality in the KC cornea including irregular fibril arrangement, reduced
305 fibril density, lamellae splitting and decreased lamella interweaving was observed in previous
306 studies (16-18, 21, 44). These microstructural changes lead to deterioration in mechanical
307 stiffness compared with the levels expected in healthy corneas (11, 45). The evident
308 association between the reduced fibril density and the stiffness deterioration has enabled the
309 development of numerical models of KC corneas that consider changes in fibril arrangement
310 (22, 23, 25, 26, 28). However, what remains lacking are methods to estimate reductions in
311 fibril density in individual eyes, which would be needed in construction of customised
312 numerical models of KC corneas. This study seeks to address this gap through developing a
313 relationship between fibril density reduction within the cone and a number of corneal features
314 including the cone area, the mean refractive power and the minimum corneal thickness. The
315 study also attempts to establish the effect of keratoconus on the density and distribution of
316 collagen fibrils outside the cone.

317 The study started with analysis of microstructure maps of 6 healthy corneas and showed that
318 the collagen fibril distribution was consistent with primarily (30.2±2.8%) of vertical fibrils and
319 (31.5±2.9%) of horizontal fibrils in the central region (up to 3 mm radius). Beyond this region,
320 the fibrils gradually change orientation, becoming more tangentially aligned with respect to the
321 edge of the cornea until the limbus (radius ≈ 5.5 mm) where the percentage of tangential fibrils
322 reaches 37.2±1.8%. Although comparative data was not available from the limbal region of
323 the KC corneas, it was noted that the fibril distribution outside the cone areas was similar to
324 that observed in healthy corneas. In KC corneas, the percentages of the vertical and horizontal
325 fibrils in the central corneas, but excluding the cone areas, were 30.8±1.5% and 30.0±1.5%,
326 respectively, with no significant differences compared to corresponding values in healthy
327 corneas (p= 0.22, 0.29).

328 The range of fibril density reduction in the cone areas of the 7 KC corneas analysed in this
329 study was between 20 and 39%. This magnitude of density loss was correlated with three

330 parameters; namely the cone area, the mean refractive power and the minimum corneal
331 thickness ($p= 0.001, 0.008, 0.041$, respectively). Another parameter, the distance between
332 corneal apex and cone centre, was excluded due to lack of significant correlation with density
333 reduction. Based on these results, an estimate of a cone fibril reduction factor κ was
334 developed and found to offer a close match with measured values. With the proven
335 dependence of corneal stiffness on collagen fibril distribution, this parameter could be
336 employed in numerical analyses to simulate the effect of KC on corneal biomechanical
337 behaviour.

338 The study has a number of limitations. First, the change in fibril alignment within the cones
339 that has been observed in some keratoconic maps was not consistent and could not be
340 quantified, and therefore could not be considered in the current study. Second, the number of
341 cornea specimens included in the study was relatively small due to the difficulty in obtaining
342 full tissue thickness KC buttons. As new data becomes available, the method developed in
343 this study will be updated.

344 In conclusion, this study presented a method to estimate the reduction in collagen fibril density
345 inside the cone areas of KC corneas. The study also presented evidence that the fibril
346 distribution outside the cone areas was not affected by KC development and progression and
347 was therefore similar to the fibril distribution in healthy corneas. These findings would make it
348 possible to develop customised numerical models that predict the biomechanical behaviour of
349 KC corneas.

350

351 **Author Contributions Statement**

352 DZ, BL and AA developed the method and drafted the paper. DZ and AEIasy performed the
353 analysis. BL contributed to the statistical analysis. SH, KM and CB collected the x-ray
354 scattering data. AA, AM, NM and AEIsheikh supervised the project. AEIsheikh designed the
355 study. All authors reviewed the manuscript.

356

357 **Acknowledgements**

358 Authors acknowledge the EPSRC grant EP/N014499/1, the MRC grants MR/S037829/1,
359 MR/K000837/1, and NIH grant R01EY021500. Authors thank the Diamond Light Source for
360 beamtime access under award numbers MX8443 and MX11316.

361

362 **Conflict of Interest Statement**

363 There is no conflict of interest to declare.

364

365 **References:**

- 366 1. Auffarth GU, Wang L, Völcker HE. Keratoconus evaluation using the Orbscan topography
367 system. *Journal of Cataract & Refractive Surgery*. 2000;26(2):222-8.
- 368 2. Montalbán R, Alió JL, Javaloy J, Piñero DP. Comparative analysis of the relationship between
369 anterior and posterior corneal shape analyzed by Scheimpflug photography in normal and
370 keratoconus eyes. *Graefe's Archive for Clinical and Experimental Ophthalmology*. 2013;251(6):1547-
371 55.
- 372 3. Tomidokoro A, Oshika T, Amano S, Higaki S, Maeda N, Miyata K. Changes in anterior and
373 posterior corneal curvatures in keratoconus. *Ophthalmology*. 2000;107(7):1328-32.
- 374 4. Alió JL, Shabayek MH. Corneal higher order aberrations: a method to grade keratoconus.
375 *Journal of Refractive Surgery*. 2006;22(6):539-45.
- 376 5. Accardo PA, Pensiero S. Neural network-based system for early keratoconus detection from
377 corneal topography. *Journal of biomedical informatics*. 2002;35(3):151-9.
- 378 6. Yousefi S, Yousefi E, Takahashi H, Hayashi T, Tampo H, Inoda S, et al. Keratoconus severity
379 identification using unsupervised machine learning. *PLoS One*. 2018;13(11):e0205998.
- 380 7. Krumeich JH, Daniel J. Lebend-Epikeratophakie und Tiefe Lamelläre Keratoplastik zur
381 Stadiengerechten chirurgischen Behandlung des Keratokonus (KK) I-III. *Klinische Monatsblätter für*
382 *Augenheilkunde*. 1997;211(08):94-100.
- 383 8. Andreassen TT, Hjorth Simonsen A, Oxlund H. Biomechanical properties of keratoconus and
384 normal corneas. *Experimental Eye Research*. 1980;31(4):435-41.
- 385 9. Scarcelli G, Besner S, Pineda R, Yun SH. Biomechanical Characterization of Keratoconus
386 Corneas Ex Vivo With Brillouin Microscopy Evaluation of Brillouin Microscopy for Keratoconus.
387 *Investigative Ophthalmology & Visual Science*. 2014;55(7):4490-5.
- 388 10. Reinstein DZ, Gobbe M, Archer TJ, Silverman RH, Coleman DJ. Epithelial, stromal, and total
389 corneal thickness in keratoconus: three-dimensional display with artemis very-high frequency digital
390 ultrasound. *Journal of Refractive Surgery*. 2010;26(4):259-71.
- 391 11. Mikula E, Winkler M, Juhasz T, Brown DJ, Shoa G, Tran S, et al. Axial mechanical and
392 structural characterization of keratoconus corneas. *Experimental Eye Research*. 2018;175:14-9.
- 393 12. Nash IS, Greene PR, Foster CS. Comparison of mechanical properties of keratoconus and
394 normal corneas. *Experimental eye research*. 1982;35(5):413-24.
- 395 13. Aghamohammadzadeh H, Newton RH, Meek KM. X-Ray Scattering Used to Map the
396 Preferred Collagen Orientation in the Human Cornea and Limbus. *Structure*. 2004;12(2):249-56.
- 397 14. Meek K. The cornea and sclera. *Collagen: structure and mechanics*. 2008:359-96.

- 398 15. Zhou D, Eliasy A, Abass A, Markov P, Whitford C, Boote C, et al. Analysis of X-ray scattering
399 microstructure data for implementation in numerical simulations of ocular biomechanical behaviour.
400 PLOS ONE. 2019;14(4):e0214770.
- 401 16. Daxer A, Fratzl P. Collagen fibril orientation in the human corneal stroma and its implication
402 in keratoconus. *Investigative ophthalmology & visual science*. 1997;38(1):121-9.
- 403 17. Meek KM, Tuft SJ, Huang Y, Gill PS, Hayes S, Newton RH, et al. Changes in collagen
404 orientation and distribution in keratoconus corneas. *Investigative ophthalmology & visual science*.
405 2005;46(6):1948-56.
- 406 18. Hayes S, Boote C, Tuft SJ, Quantock AJ, Meek KM. A study of corneal thickness, shape and
407 collagen organisation in keratoconus using videokeratography and X-ray scattering techniques.
408 *Experimental Eye Research*. 2007;84(3):423-34.
- 409 19. Radner W, Zehetmayer M, Skorpik C, Mallinger R. Altered organization of collagen in the
410 apex of keratoconus corneas. *Ophthalmic research*. 1998;30(5):327-32.
- 411 20. Morishige N, Wahlert AJ, Kenney MC, Brown DJ, Kawamoto K, Chikama T-i, et al. Second-
412 Harmonic Imaging Microscopy of Normal Human and Keratoconus Cornea. *Investigative*
413 *Ophthalmology & Visual Science*. 2007;48(3):1087-94.
- 414 21. Dawson DG, Randleman JB, Grossniklaus HE, O'Brien TP, Dubovy SR, Schmack I, et al. Corneal
415 Ectasia After Excimer Laser Keratorefractive Surgery: Histopathology, Ultrastructure, and
416 Pathophysiology. *Ophthalmology*. 2008;115(12):2181-91.e1.
- 417 22. Pinsky PM, van der Heide D, Chernyak D. Computational modeling of mechanical anisotropy
418 in the cornea and sclera. *Journal of Cataract & Refractive Surgery*. 2005;31(1):136-45.
- 419 23. Studer H, Larrea X, Riedwyl H, Büchler P. Biomechanical model of human cornea based on
420 stromal microstructure. *Journal of biomechanics*. 2010;43(5):836-42.
- 421 24. Pandolfi A, Manganiello F. A model for the human cornea: constitutive formulation and
422 numerical analysis. *Biomechanics and modeling in mechanobiology*. 2006;5(4):237-46.
- 423 25. Pandolfi A, Holzapfel GA. Three-dimensional modeling and computational analysis of the
424 human cornea considering distributed collagen fibril orientations. *Journal of biomechanical*
425 *engineering*. 2008;130(6):061006.
- 426 26. Whitford C, Studer H, Boote C, Meek KM, Elsheikh A. Biomechanical model of the human
427 cornea: Considering shear stiffness and regional variation of collagen anisotropy and density. *Journal*
428 *of the mechanical behavior of biomedical materials*. 2015;42:76-87.
- 429 27. Pijanka JK, Abass A, Sorensen T, Elsheikh A, Boote C. A wide-angle X-ray fibre diffraction
430 method for quantifying collagen orientation across large tissue areas: application to the human
431 eyeball coat. *Journal of Applied Crystallography*. 2013;46(5):1481-9.
- 432 28. Zhou D, Abass A, Eliasy A, Studer HP, Movchan A, Movchan N, et al. Microstructure-based
433 numerical simulation of the mechanical behaviour of ocular tissue. *Journal of The Royal Society*
434 *Interface*. 2019;16(154):20180685.
- 435 29. Hayes S, Boote C, Tuft SJ, Quantock AJ, Meek KM. A study of corneal thickness, shape and
436 collagen organisation in keratoconus using videokeratography and X-ray scattering techniques.
437 *Experimental Eye Research Journal*. 2007;84(3):423-34.
- 438 30. Boote C, Dennis S, Huang Y, Quantock AJ, Meek KM. Lamellar orientation in human cornea in
439 relation to mechanical properties. *J Struct Biol*. 2005;149(1):1-6.
- 440 31. Sadoughi MM, Einollahi B, Einollahi N, Rezaei J, Roshandel D, Feizi S. Measurement of central
441 corneal thickness using ultrasound pachymetry and Orbscan II in normal eyes. *Journal of ophthalmic*
442 *& vision research*. 2015;10(1):4.
- 443 32. Rainer G, Findl O, Petternel V, Kiss B, Drexler W, Skorpik C, et al. Central corneal thickness
444 measurements with partial coherence interferometry, ultrasound, and the Orbscan system.
445 *Ophthalmology*. 2004;111(5):875-9.
- 446 33. Dutta D, Rao HL, Addepalli UK, Vaddavalli PK. Corneal thickness in keratoconus: comparing
447 optical, ultrasound, and optical coherence tomography pachymetry. *Ophthalmology*.
448 2013;120(3):457-63.

- 449 34. Mahmoud AM, Roberts CJ, Lembach RG, Twa MD, Herderick EE, McMahon TT. CLMI: the
450 cone location and magnitude index. *Cornea*. 2008;27(4):480-7.
- 451 35. Eliasy A, Abass A, Lopes BT, Vinciguerra R, Zhang H, Vinciguerra P, et al. Characterization of
452 cone size and centre in keratoconic corneas. *Journal of The Royal Society Interface*.
453 2020;17(169):20200271.
- 454 36. Olsen T. On the calculation of power from curvature of the cornea. *The British Journal of*
455 *Ophthalmology*. 1986;70(2):152-4.
- 456 37. Ho J-D, Tsai C-Y, Tsai RJ-F, Kuo L-L, Tsai IL, Liou S-W. Validity of the keratometric index:
457 Evaluation by the Pentacam rotating Scheimpflug camera. *Journal of Cataract & Refractive Surgery*.
458 2008;34:137-45.
- 459 38. Abass A, Clamp J, Bao F, Ambrosio R, Jr., Elsheikh A. Non-Orthogonal Corneal Astigmatism
460 among Normal and Keratoconic Brazilian and Chinese populations. *Curr Eye Res*. 2018:1-8.
- 461 39. Smit G, Atchison DA. *The eye and visual optical instruments*: Cambridge University Press;
462 1970.
- 463 40. Vojnikovi Bo, Tamajo E. Gullstrand's Optical Schematic System of the Eye Modified by
464 Vojnikovi & Tamajo. *Coll Antropol*. 2013;37 (1):41-5.
- 465 41. Abass A, Lopes BT, Eliasy A, Wu R, Jones S, Clamp J, et al. Three-dimensional non-parametric
466 method for limbus detection. *PLOS ONE*. 2018;13(11):e0207710.
- 467 42. Abass A, Lopes BT, Eliasy A, Salomao M, Wu R, White L, et al. Artefact-free topography based
468 scleral-asymmetry. *PLOS ONE*. 2019;14(7):e0219789.
- 469 43. Renka RJ, Renka RL, Cline AK. A TRIANGLE-BASED C^1 INTERPOLATION METHOD. *The Rocky*
470 *Mountain Journal of Mathematics*. 1984;14(1):223-37.
- 471 44. Mathew JH, Goosey JD, Söderberg PG, Bergmanson JP. Lamellar changes in the keratoconic
472 cornea. *Acta ophthalmologica*. 2015;93(8):767-73.
- 473 45. Gefen A, Shalom R, Elad D, Mandel Y. Biomechanical analysis of the keratoconic cornea.
474 *Journal of the Mechanical Behavior of Biomedical Materials*. 2009;2(3):224-36.
- 475